Flexible Fibrils

DOI: 10.1002/anie.200904781

Nanoscale Flexibility Parameters of Alzheimer Amyloid Fibrils Determined by Electron Cryo-Microscopy**

*Carsten Sachse, Nikolaus Grigorieff, and Marcus Fändrich**

Amyloid fibrils are fibrillar polypeptide aggregates consisting of a cross-β structure.[1,2] The rigidity and stability of these fibrils contributes to their natural pathogenicity or functionality and has suggested potential applications in bionanotechnology.[3–6] Yet, amyloid fibrils can occur in different morphologies with unique mechanical and flexible characteristics.[7–9] Herein, we use electron cryo-microscopy (cryo-EM) to characterize these nanoscale structural properties. Cryo-EM images effectively represent snapshots of thermally fluctuating fibrils in solution; it is not necessary to micromanipulate or immobilize the fibrils on a solid surface. The amyloid fibrils analyzed here consist of Alzheimer's Aβ(1–40) peptide. They are homogenous in width ($w \approx 20$ nm), although different fibrils can vary significantly in their crossover distances d (Figure 1).

In addition to these interfibrillar differences, there are variations of d within each single fibril. However, the intrafibrillar standard deviations of d range mostly from 5 to 7 nm, while average d values of different fibrils vary from 100 to 160 nm (Figure 2 A). Hence, the encountered variations cannot be explained by purely thermally determined and stochastic fluctuations. Instead, they represent subtle, yet systematic, structural differences between the fibrils in the sample.

To further analyze these structural differences, two subpopulations were defined, termed here F120 and F140 fibrils. F140 fibrils show mean d values of (140 ± 10) nm (Figure 2 B), and their 3D structure was reconstructed previously at approximately 8 Å resolution.[10,11] F120 fibrils possess an average d value of (120 ± 10) nm (Figure 2 B). The structure of F120 fibrils is determined here at approximately 10 Å resolution (Figure 3 A, B, Figure 2 in the Supporting Information). Whereas the distinction between F120 and

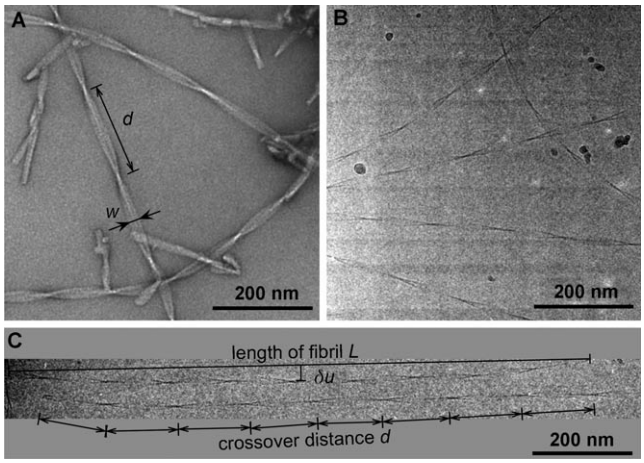

Figure 1. Global structural characteristics. Negatively stained micrographs (A) and cryo-micrographs (B, C) illustrate definitions of fibril length L, width w, crossover distance d, and normal distance δu.

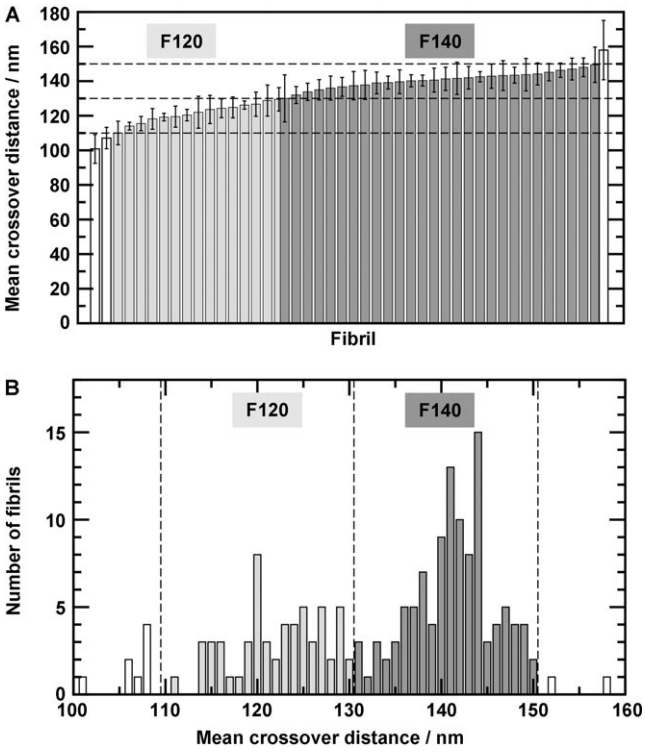

Figure 2. A) Mean crossover distances of representative fibrils. B) Distribution of mean crossover distances of the entire fibril population. F120: light gray; F140: dark gray.

[*] M. Fändrich
Max-Planck Research Unit for Enzymology of Protein Folding and Martin-Luther University Halle-Wittenberg
Weinbergweg 22, 06120 Halle an der Saale (Germany)
E-mail: fandrich@enzyme-halle.mpg.de
C. Sachse
MRC Laboratory of Molecular Biology, Cambridge, (UK)
N. Grigorieff
Rosenstiel Basic Medical Sciences Research Center and Howard Hughes Medical Institute
Brandeis University, Waltham, MA (USA)

[**] This research was supported by the BMBF (BioFuture, grant to M.F.) and the DFG (SFB 610, grant to M.F.), the National Institutes of Health (grant 1 P01 GM-62580 to N.G.), and by EMBO (long-term postdoctoral fellowship for C.S.).

Supporting information for this article is available on the WWW under http://dx.doi.org/10.1002/anie.200904781.

© 2010 Wiley-VCH Verlag GmbH & Co. KGaA, Weinheim

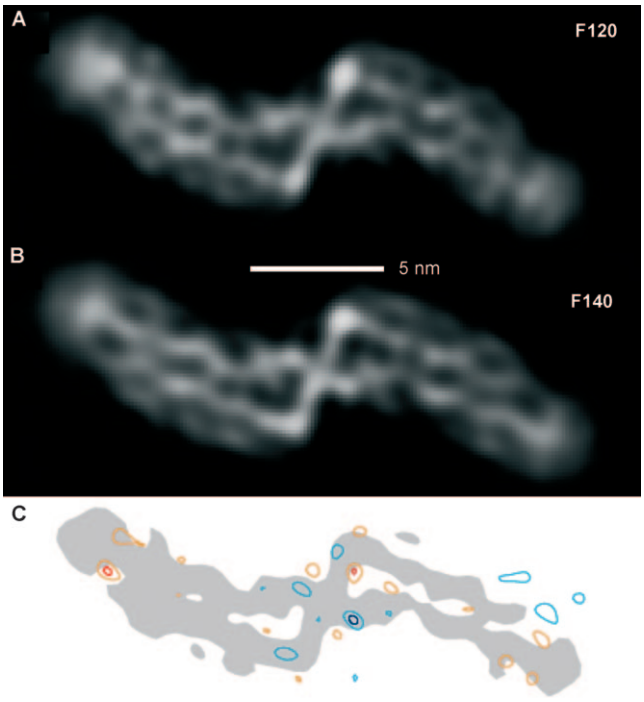

Figure 3. Cross-section of F120 (A) and F140 fibrils (B). C) Difference map F140−F120. Negative peaks: orange = 2σ, red = 3σ. Positive peaks: light blue = 2σ, blue = 3σ.

F140 fibrils remains arbitrary, the two subpopulations consist of a sufficiently large data set for a medium-resolution 3D reconstruction and for measurement of the nanoscale elastic properties. Reconstructed F120 and F140 fibrils present effectively the same cross-section (Figure 3). Hence, the conformational differences of the peptides forming F120 and F140 fibrils are too small to be revealed at the current levels of structural resolution. These data imply that the systematic variations in the crossover distances of different fibrils (Figure 2 A) occur within fibrils that all belong to the same basic morphology. In other words, different fibrils of the same morphology can occur with different torsional properties.

Calculation of the nanoscale elastic properties is based on the measurement of variations of fibril twisting and bending. Assuming that the fibrils are made up of an isotropic homogeneous medium, variations of the fibril twist d enable computation of torsional persistence length l_c and torsional rigidity c. Bending variations yield persistence length l_p and bending rigidity κ (see the Supporting Information for details). Our measurements imply that F120 and F140 fibrils possess very similar, if not identical, torsional properties (torsional rigidity c and torsional persistence length l_c; Table 2 in the Supporting Information). By contrast, the two fibril populations differ significantly in their bending properties (Table 3 in the Supporting Information). F120 fibrils possess a smaller bending rigidity κ (Table 3 in the Supporting Information) and a larger normalized bending fluctuation Δu than F140 fibrils (Figure 3 B in the Supporting Information). However, part of this difference may result from the different spacing of crossovers in these two populations (Figure 3 in the Supporting Information).

The measured l_p and κ values are within the reported range for other amyloid fibrils.[12–14] They also comply with a fundamental relationship between l_p and the molecular density (mass per length; Figure 4 A).

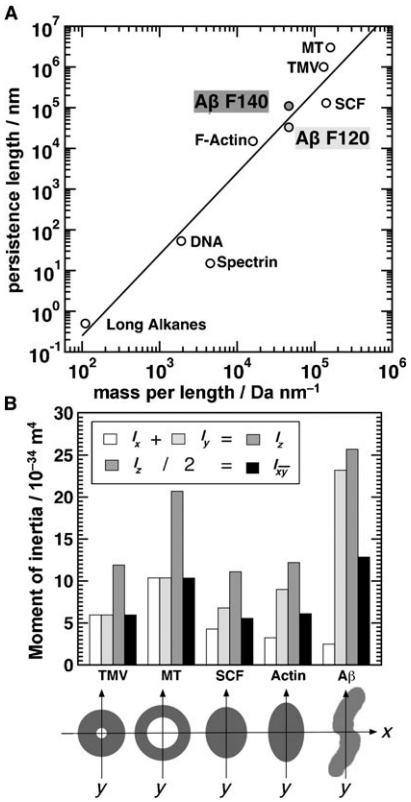

Figure 4. Flexibility parameters of F120 and F140 fibrils in comparison with those of other filamentous protein assemblies. A) Persistence length increases with the increase in mass per unit of length.[19] B) Comparison of moments of inertia and polar moments of inertia from models of area-normalized cross-sections of different protein filaments. TMV: tobacco mosaic virus, MT: microtubules, SCF: sickle-cell hemoglobin fibers.

For several protein fibrils, the dependence of c and κ on shape- and material-specific factors has been analyzed.[15–17] The physical formalism used in these analyses was developed for macroscopic objects. Thus, its general applicability to nanoscale protein fibrils remains to be established. According to this formalism, the torsional rigidity c depends on the shape-dependent polar moment of inertia I_z and the material-specific shear modulus G [Eq. (1)]. The bending rigidity κ depends on the material-specific Young's modulus Y and the shape-dependent moment of inertia $I_{\overline{xy}}$ [Eq. (2)].

$$c = I_z G \tag{1}$$

$$\kappa = I_{\overline{xy}} Y \tag{2}$$

In contrast to previous approaches that had to use model estimates for the fibril cross-section, cryo-EM enables calcu-

 © 2010 Wiley-VCH Verlag GmbH & Co. KGaA, Weinheim

lation of the two shape-dependent factors I_z and $I_{\overline{xy}}$ directly from the cross-section of the 3D fibril reconstructions. F120 and F140 fibrils effectively possess the same cross-sectional architecture (Figure 3) and therefore similar shape-specific factors I_z and $I_{\overline{xy}}$ (Tables 2 and 3 in the Supporting Information). The torsional rigidities of F120 and F140 fibrils are very similar and produce the same shear modulus G within error margins [Eq. (1), Table 2 in the Supporting Information).

We have compared the calculated material moduli with literature data. Exact numeric values should be considered carefully, however, owing to possible effects of the method of analysis.[14] The shear moduli G of F120 and F140 fibrils (12.7 MPa) are in close proximity to those of other protein assemblies, such as F-actin (9 MPa)[16] and sickle-cell fibrils (SCF, 1 MPa).[18] In comparison to macroscopic materials, these values fall in the range between plastics (ca. 100 MPa) and rubber (ca. 0.6 MPa).[19] The Young's moduli Y of F120 and F140 fibrils (90 and 320 MPa, respectively) are close to the observed values for filamentous proteins, such as SCF (50 MPa),[18] but are somewhat lower than figures of microtubuli and actin (1 and 3 GPa, respectively).[15]

The material constants of F120 and F140 fibrils differ more profoundly from those reported recently for insulin amyloid fibrils (shear modulus $G = 130$ MPa, Young's modulus $Y = 6$ GPa[14]). By contrast, the persistence length (42 μm) and bending rigidity (1.7×10^{-25} N m^2) of insulin fibrils are remarkably similar to those of Aβ(1–40) fibrils. Since no 3D reconstruction of the analyzed insulin fibrils was reported, their cross-sectional structure cannot be compared easily with the structure of the Aβ(1–40) fibrils used here.

While our data cannot confirm the existence of unusually high nanoscale material constants for the analyzed Aβ(1–40) fibrils, we find that the shape-dependent properties polar moment of inertia I_z and moment of inertia $I_{\overline{xy}}$ are significantly greater for the analyzed Aβ(1–40) fibrils than for area-normalized cross-sections of other protein filaments (Figure 4B). Hence, the analyzed Aβ fibrils represent a very material-efficient way to construct proteinaceous filaments of high stability and structural flexibility. These observations are relevant for better estimating the potential applications of amyloid fibrils in the material sciences.

In addition, our data contribute to understanding amyloid pathogenicity in vivo. The stability and flexibility of amyloid fibrils are similar to those of native protein filaments, such as F-actin or microtubules. However, growth and disassembly of the latter represent highly dynamic and regulated processes, and as such they are tightly controlled by specific sets of proteins. Therefore, an unregulated outgrowth of similarly stable amyloid fibrils will be much more difficult to tolerate within a biological environment. This conclusion is consistent with the fact that amyloid pathogenicity arises, at least partially, from the distortion or disruption of naturally elastic and flexible tissues, such as cardiac ventricles or blood vessel walls.[20] Further work will be required, however, to delineate the cellular pathways by which these reactions result in the death of affected cells.

Received: August 26, 2009
Revised: November 13, 2009
Published online: January 12, 2010

Keywords: Alzheimer's disease · amyloids · electron microscopy · nanotechnology · protein folding

[1] R. Jansen, W. Dzwolak, R. Winter, *Biophys. J.* **2005**, *88*, 1344–1353.
[2] L. C. Serpell, *Biochim. Biophys. Acta Mol. Basis Dis.* **2000**, *1502*, 16–30.
[3] I. Cherny, E. Gazit, *Angew. Chem.* **2008**, *120*, 4128–4136; *Angew. Chem. Int. Ed.* **2008**, *47*, 4062–4069.
[4] Y. Goto, H. Yagi, K. Yamaguchi, E. Chatani, T. Ban, *Curr. Pharm. Des.* **2008**, *14*, 3205–3218.
[5] D. Otzen, P. H. Nielsen, *Cell. Mol. Life Sci.* **2008**, *65*, 910–927.
[6] G. Tuchscherer, A. Chandravarkar, M. S. Camus, J. Bérard, K. Murat, A. Schmid, R. Mimna, H. A. Lashuel, M. Mutter, *Biopolymers* **2007**, *88*, 239–252.
[7] M. Fändrich, J. Meinhardt, N. Grigorieff, *Prion* **2009**, *3*, 89–93.
[8] J. Meinhardt, C. Sachse, P. Hortschansky, N. Grigorieff, M. Fändrich, *J. Mol. Biol.* **2009**, *386*, 869–877.
[9] R. Wetzel, S. Shivaprasad, A. D. Williams, *Biochemistry* **2007**, *46*, 1–10.
[10] C. Sachse, M. Fändrich, N. Grigorieff, *Proc. Natl. Acad. Sci. USA* **2008**, *105*, 7462–7466.
[11] C. Sachse, C. Xu, K. Wieligmann, S. Diekmann, N. Grigorieff, M. Fändrich, *J. Mol. Biol.* **2006**, *362*, 347–354.
[12] T. P. Knowles, A. W. Fitzpatrick, S. Meehan, H. R. Mott, M. Vendruscolo, C. M. Dobson, M. E. Welland, *Science* **2007**, *318*, 1900–1903.
[13] T. P. Knowles, J. F. Smith, A. Craig, C. M. Dobson, M. E. Welland, *Phys. Rev. Lett.* **2006**, *96*, 238301.
[14] J. F. Smith, T. P. Knowles, C. M. Dobson, C. E. Macphee, M. E. Welland, *Proc. Natl. Acad. Sci. USA* **2006**, *103*, 15806–15811.
[15] F. Gittes, B. Mickey, J. Nettleton, J. Howard, *J. Cell Biol.* **1993**, *120*, 923–934.
[16] E. Prochniewicz, N. Janson, D. D. Thomas, E. M. De La Cruz, *J. Mol. Biol.* **2005**, *353*, 990–1000.
[17] J. C. Wang, M. S. Turner, G. Agarwal, S. Kwong, R. Josephs, F. A. Ferrone, R. W. Briehl, *J. Mol. Biol.* **2002**, *315*, 601–612.
[18] M. S. Turner, R. W. Briehl, J. C. Wang, F. A. Ferrone, R. Josephs, *J. Mol. Biol.* **2006**, *357*, 1422–1427.
[19] D. Boal, *Mechanics of the Cell*, Cambridge University Press, **2002**.
[20] M. B. Pepys, *Annu. Rev. Med.* **2006**, *57*, 223–241.

 © 2010 Wiley-VCH Verlag GmbH & Co. KGaA, Weinheim

Angewandte Chemie
Eine Zeitschrift der Gesellschaft Deutscher Chemiker

Supporting Information

© Wiley-VCH 2010

69451 Weinheim, Germany

Nanoscale Flexibility Parameters of Alzheimer Amyloid Fibrils Determined by Electron Cryo-Microscopy**

*Carsten Sachse, Nikolaus Grigorieff, and Marcus Fändrich**

anie_200904781_sm_miscellaneous_information.pdf

Sample preparation and electron cryo-microscopy

Chemically synthetic Aβ(1-40) (Bachem) was dissolved at 5mg/ml concentration in water and snap-frozen in aliquots. To induce fibril formation, one aliquot was thawn and diluted using a 750 mM sodium borate pH 7.8 stock solution to a final concentration of 1 mg/ml peptide at 50 mM borate. The final pH-value obtained upon dilution was 8.7. Fibrils were grown for a minimum of four days and plunge-frozen in the coldroom[1]. An FEI F30 cryo-microscope was operated at 300 kV under low-dose conditions and specimens were imaged on Kodak ISO163 film at a nominal magnification of 59,000.

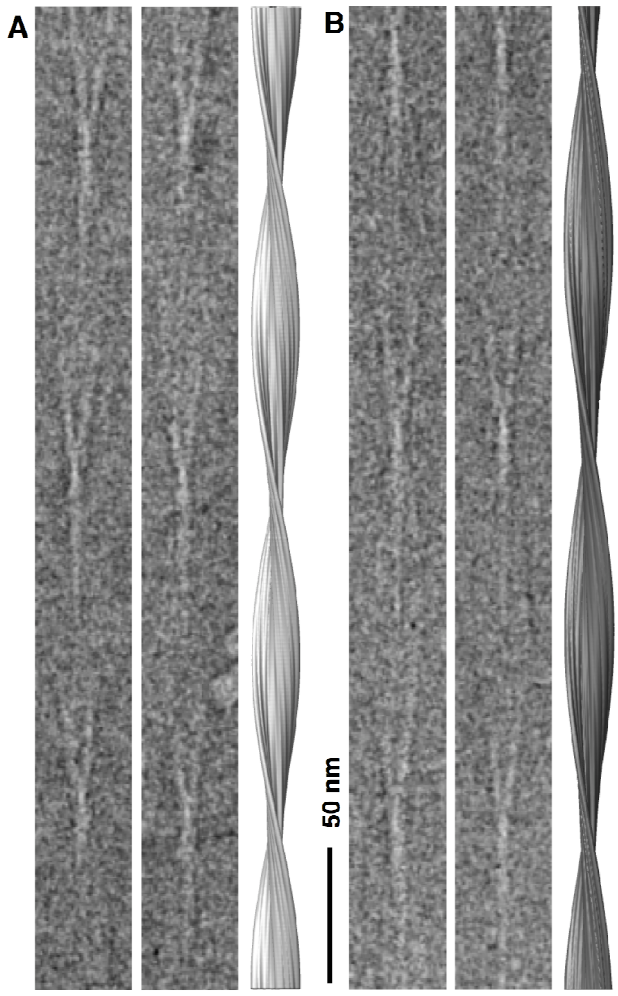

Supp. Figure 1. Three-dimensional image reconstruction of Aβ(1-40) amyloid fibrils. (A) and (B) Examples of two straight fibrils from each population included in the image reconstruction. Surface-rendered side view of F120 (light grey) and F140 (dark grey) reconstruction.

Image processing and 3D image reconstruction

We selected 60 micrographs from a total of 250 according to image and fibril quality, and subsequently scanned them on a Zeiss SCAI scanner with a raster size of 7 µm[1]. We assessed fibril homogeneity by measuring their width and crossover distance using JMicrovision software[2]. In addition to the previously reconstructed population with crossover distances between 130 and 150 nm (F140 population), we define an additional subpopulation characterized by crossover distances between 110 and 130 nm (F120 population). These fibrils were processed in the same way as the previous fibril reconstruction[1]. Fibrils were segmented using EMAN's BOXER[3]. Image processing was performed using the SPIDER software package[4] as described[1, 5]. As a first reference model, we chose a cylinder and obtained a second 3D structure of an Aβ(1-40) amyloid fibril from the F120 subset at a resolution of ~10 Å (image processing statistics are summarized in Supp. Table 1) (Supp. Figure 1A and 2). In addition, we also tested the F140 structure as a reference structure, which gave rise to a very similar cross-section (data not shown).

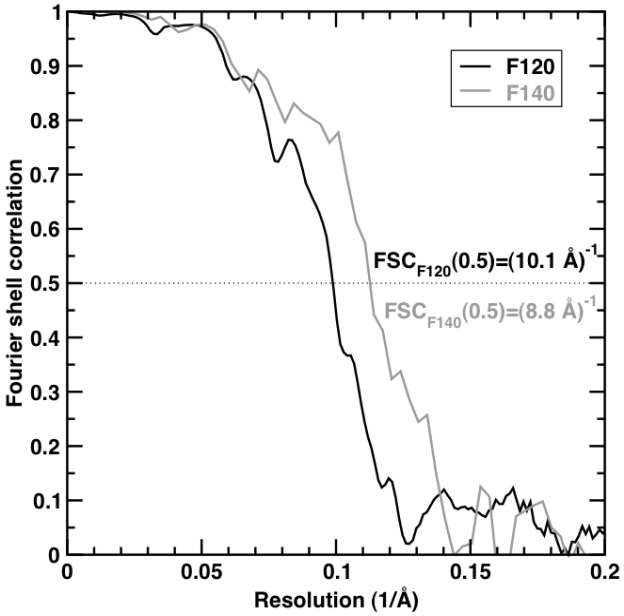

Supp Figure 2. Resolution assessment of F120 and F140 fibril populations. Fourier-shell correlation between two halves of the datasets are compared. F120 has been determined at a resolution of ~10 Å. Data for F140 fibrils were taken from Sachse et al.[1]

We compared the two subpopulations F120 and F140 by difference mapping. First, we aligned the two cross-sectional slices of the F120 and F140 reconstruction, and subsequently normalized their densities and finally subtracted F120 from F140 (Figure 3C).

Supp. Table 1. Image processing statistics of two Aβ(1-40) fibril populations. Data for F140 fibrils were taken from Sachse et al.[1]

Fibril population	F120	F140
Resolution at FSC 0.5/0.143 (Å)	10.1/8.7	8.8/7.1
Total length of non-overlapping segments (nm)	43,160	87,265
Number of fibrils	58	188
Number of segments	6129	11527
Segment size (nm)	84.2	84.2
Size of 3D reconstruction (nm)	77.7	77.7
Segment step size (nm)	6.3	6.3
Average crossover distance/repeat distance (nm)	121.0/0.48	142.5 / 0.48
Pixel size on the specimen (Å)	2.4	1.2

Determination of polar moment of inertia and moment of inertia

a. Polar moment of inertia

With the knowledge of the 3D fibril structure, we can estimate the resistance against torsional stress arising from the cross-sectional structure. Thus, we computed the polar moment of inertia I_z of the cross-section excised from the 3D fibril cryo-EM reconstruction:

$$I_z = \int r^2 dA \qquad \text{(Supp. Eq. 1).}$$

where r is the radial distance and A is the cross-sectional area of a pixel. To evaluate the integral, the 3D reconstructions of F120 and F140 were filtered to a resolution of 20 Å to smooth the rendering of the cross-sectional density. Then, we converted the cross-sections into binary masks at the threshold of 3 x sigma. For each pixel with a density of one, we calculated the radial distance to the center of the cross-section, squared the distances and multiplied by the elemental pixel area of 1.2 x 1.2 Å. Finally, these products were added to yield the polar moment of inertia.

b. Moment of inertia

The cross-sectional shape confers resistance against bending deformation, which is dependent on the axis where the force is applied. The moments of inertia I_x and I_y are defined as:

$$I_x = \int y^2 dA \qquad \text{(Supp. Eq. 2)}$$

and

$$I_y = \int x^2 dA \qquad \text{(Supp. Eq. 3)}$$

where y and x represent the distances of a pixel with area dA to the x- and y-axis, respectively (Figure 4B). Since Aβ(1-40) fibrils exhibit a regular twist, this directional dependence will be averaged over the course of a single crossover to:

$$I_{\overline{xy}} = \frac{I_x + I_y}{2} \qquad \text{(Supp. Eq. 4).}$$

For the polar moment of inertia, we calculated the distance r to the fibril axis, squared them and multiplied by the elemental pixel area of 1.2 x 1.2 Å. We used the same binary mask to calculate both moments. In agreement with Supp. Eq. 1 and Supp. Eq. 4, $I_{\overline{xy}}$ reduces to half of I_z.

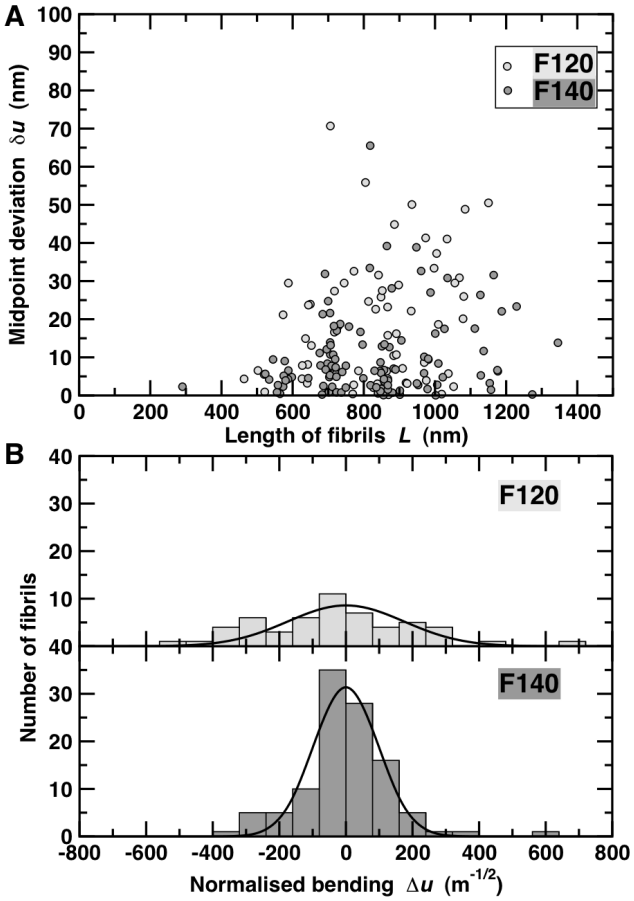

Supp. Figure 3. Flexibility analysis of 178 fibrils. Bending analysis. (A) Parameters of fibril length and corresponding midpoint deviation were measured for the two subpopulations F120 and F140 and plotted in a scatter diagram. (B) Two histograms of length-normalized bending were derived from the previous measurements of the two subpopulations and the entire population and subsequently fitted with Gaussian curves of a standard deviation of 174 and 96 $m^{1/2}$ respectively. While the different bending properties of F120 and F140 fibrils are statistically significant, this difference may be due to the flattened cross-sections of these fibrils. Since the bending of the fibrils is limited to the two-dimensional plane of the ice layer, it cannot be excluded that bending occurs predominantly at crossovers, i.e. where the flat side of a fibril is oriented perpendicular to the ice layer (Figure 1C). As a result, fibrils with a shorter crossover distances could possess a higher susceptibility to bending than fibrils with longer crossover distances.

Flexibility analysis

A previous flexibility analysis on sickle-cell hemoglobin fibers based on raw cryo-EM images was proposed by Turner and co-workers[6]. The analysis assumes that fibrils consist of an isotropic and homogeneous material. In analogy, we determined twisting and bending parameters of Aβ(1-40) amyloid fibrils.

a. Torsion analysis

Supp. Table 2. Torsional properties of Aβ(1-40) fibrils

Fibril population	F120*	F140*
Crossover distance, *d,* range [nm]	110 - 130	130 – 150
Averaged mean crossover distance, *d* ± averaged standard deviation s_d [nm]	122 ± 5.6	141 ± 7.0
Torsional persistence length, l_c [10^{-6} m]	9.3 (0.3)	8.6 (0.1)
Torsional rigidity, *c* [10^{-26} Nm^2]	3.5 (0.1)	3.3 (0.1)
Polar moment of inertia, I_z [10^{-33} m^4]	2.8 (0.9)	2.6 (0.8)
Shear modulus, *G* [MPa]	12.7 (2.6)	12.7 (2.7)

* error in parentheses

The distribution of crossover distances *d* provides information on the internal torsional properties of the fibrils. Therefore, crossover distance measurements were taken from 60 digitized micrographs using JMicrovision software[2] (Figure 1C). In order to minimize measurement errors, we included only those fibrils with more than six crossovers in the flexibility analysis. Finally, we took a total of 1180 measurements from 178 fibrils and calculated the mean crossover distance of each individual fibril and their corresponding standard deviation. The analysis revealed that the crossover distance variation within a single fibril is significantly smaller than the variation present in the entire fibril population (Figure 2A). As a result of the subdivision of the fibril population, the F120 dataset contained 58 fibrils, the F140 dataset consisted of 110 fibrils (Figure 2B) and 10 fibrils outside the analyzed crossover range were discarded. According to Turner et al., 2006[6], we obtain the torsional persistence length l_c of each fibril:

$$l_c = \frac{d^3}{\left(s_d\right)^2 \cdot \pi^2} \qquad \text{(Supp. Eq. 5).}$$

Finally, we averaged the torsional persistence length of F120 and F140 fibril members. Their torsional rigidity *c* can be determined as:

$$c = l_c \cdot k_B \cdot T \qquad \text{(Supp. Eq. 6),}$$

where k_B is the Boltzmann constant (1.381×10^{-23} Nm/K), *T* the temperature of the sample. Therefore, l_c and *c* describe the resistance of fibril structures towards torsional deformations.

For a uniform elastic medium, the shear modulus *G* represents a material-specific constant characterizing its intrinsic twisting ability is dependent on the ratio of torsional rigidity *c* and the polar moment of inertia I_z:

$$G = \frac{c}{I_z} \qquad \text{(Supp. Eq. 7).}$$

We display the figures used for the torsional analysis in the abovementioned equations in Supp. Table 2 calculated for fibril subpopulations F120 and F140. We obtained similar figures when fibrils are subdivided into four subpopulations.

b. Bending analysis

Supp. Table 3. Bending properties of Aβ(1-40) fibrils

Fibril population	F120*	F140*
Normalized bending fluctuation, $s_{\Delta u}$ [$m^{-1/2}$]	174.3 (20.0)	96.1 (19.8)
Persistence length, l_p [10^{-6} m]		
	33 (1)	108 (3)
Bending rigidity, κ [10^{-25} Nm^2]	1.3 (0.06)	4.1 (0.2)
Moment of inertia, I_{xy}^{-} [10^{-33} m^4]		
lower and upper bounds	0.3 – 2.5	0.3 - 2.3
average	1.4 (0.5)	1.3 (0.5)
Young's modulus, Y [MPa]		
lower and upper bounds	50 – 443	178 – 1,620
average	90 (36)	320 (124)

* error in parentheses

The bending of fibrils correlates with its path deviation at fibril midpoint δu from the distance or length L that connects the two fibril ends (Figure 1C). In the analysis, we did not take into account out-of-the-plane fibril bending because of the confined fibril embedding in the ice layer and the small specimen tilt that we determined at ±12° using CTFTILT[7]. We measured the length L and midpoint deviation δu from the 178 fibrils; graphical analysis of these data pairs confirms that longer midpoint deviations are more commonly found in longer fibrils (Supp. Figure 3A). In analogy to Turner and co-workers[6, 8], we computed length-normalized bending fluctuations Δu for each subpopulation F120 and F140 (Supp. Figure 3B) according to:

$$\Delta u = \frac{4\sqrt{3}}{L^{\frac{3}{2}}}\delta u \qquad \text{(Supp. Eq. 8).}$$

Since these thermal bending fluctuations are Gaussian distributed, the reciprocal of the mean squared deviation $(s_{\Delta u})^2$ corresponds to the persistence length l_p.

$$l_{p(3D)} = \frac{1}{\left(s_{\Delta u}\right)^2} \qquad \text{(Supp. Eq. 9).}$$

Hence the bending rigidity κ is given by:

$$\kappa = l_p \cdot k_B \cdot T \qquad \text{(Supp. Eq. 10).}$$

Therefore, l_p and κ reflect the resistance of fibrils towards bending. We calculated the material constant describing the resistance against bending or Young's modulus Y by the ratio of the bending rigidity κ and the cross-sectional moment of inertia I_{xy}^{-}:

$$Y = \frac{\kappa}{I_{xy}^{-}} \qquad \text{(Supp. Eq. 11).}$$

The figures used in the aforementioned equations characterizing the bending properties are summarized in Supp. Table 3. Because of the high anisotropy in cross section, we also estimated lower and upper bounds of the Young's modulus using I_x and I_y as the cross-sectional moment of inertia (Supp. Table 3). We estimated the errors in Supp. Table 2 and 3 according to the laws of error propagation and assumed a primary measurement error of 2 nm.

[1] C. Sachse, M. Fändrich & N. Grigorieff, *Proc. Natl. Acad. Sci. U.S.A.* **2008**, Paired beta-sheet structure of an Abeta(1-40) amyloid fibril revealed by electron microscopy, 105, 7462-7466.
[2] N. Roduit, *Geophysical Research Abstracts* **2006**, Quantification and measurement in digital images of thin sections with JMicroVision,
[3] S. J. Ludtke, P. R. Baldwin & W. Chiu, *J Struct Biol* **1999**, EMAN: semiautomated software for high-resolution single-particle reconstructions, 128, 82-97.
[4] J. Frank, M. Radermacher, P. Penczek, J. Zhu, Y. Li, M. Ladjadj & A. Leith, *J Struct Biol* **1996**, SPIDER and WEB: processing and visualization of images in 3D electron microscopy and related fields, 116, 190-199.
[5] C. Sachse, J. Z. Chen, P. D. Coureux, M. E. Stroupe, M. Fändrich & N. Grigorieff, *J. Mol. Biol.* **2007**, High-resolution electron microscopy of helical specimens: a fresh look at tobacco mosaic virus, 371, 812-835.
[6] M. S. Turner, R. W. Briehl, J. C. Wang, F. A. Ferrone & R. Josephs, *J. Mol. Biol.* **2006**, Anisotropy in sickle hemoglobin fibers from variations in bending and twist, 357, 1422-1427.
[7] J. A. Mindell & N. Grigorieff, *J Struct Biol* **2003**, Accurate determination of local defocus and specimen tilt in electron microscopy, 142, 334-347.
[8] J. C. Wang, M. S. Turner, G. Agarwal, S. Kwong, R. Josephs, F. A. Ferrone & R. W. Briehl, *J. Mol. Biol.* **2002**, Micromechanics of isolated sickle cell hemoglobin fibers: bending moduli and persistence lengths, 315, 601-612.
[9] J. F. Smith, T. P. Knowles, C. M. Dobson, C. E. Macphee & M. E. Welland, *Proc. Natl. Acad. Sci. U.S.A.* **2006**, Characterization of the nanoscale properties of individual amyloid fibrils, 103, 15806-15811.